Journal of Zhejiang University-SCIENCE B (Biomedicine & Biotechnology) *2024 25(6):499-512*
www.jzus.zju.edu.cn; www.springer.com/journal/11585
E-mail: jzus_b@zju.edu.cn

Research Article

https://doi.org/10.1631/jzus.B2300479

Check for updates

Hemodialysis bilayer bionic blood vessels developed by the mechanical stimulation of hepatitis B viral X (*HBX*) gene-transfected hepatic stellate cells

Hongyi LIU[1,2*], Yuanyuan ZHOU[1,2*✉], Peng GUO[1], Xiongwei ZHENG[2], Weibin CHEN[1,2], Shichao ZHANG[2], Yu FU[1,2], Xu ZHOU[1], Zheng WAN[1], Bin ZHAO[3], Yilin ZHAO[1,2,4,5✉]

[1]*Department of Oncology and Vascular Interventional Radiology, Zhongshan Hospital Affiliated to Xiamen University, School of Medicine, Xiamen University, Xiamen 361004, China*
[2]*School of Medicine, Xiamen University, Xiamen 361102, China*
[3]*Xiamen Health and Medical Big Data Center, Xiamen 361008, China*
[4]*Fujian Provincial Key Laboratory of Chronic Liver Disease and Hepatocellular Carcinoma (Zhongshan Hospital Affiliated to Xiamen University), Xiamen 361004, China*
[5]*Xiamen Key Laboratory of Cellular Intervention and Interventional Medical Materials, Xiamen 361004, China*

Abstract: Artificial vascular graft (AVG) fistula is widely used for hemodialysis treatment in patients with renal failure. However, it has poor elasticity and compliance, leading to stenosis and thrombosis. The ideal artificial blood vessel for dialysis should replicate the structure and components of a real artery, which is primarily maintained by collagen in the extracellular matrix (ECM) of arterial cells. Studies have revealed that in hepatitis B virus (HBV)-induced liver fibrosis, hepatic stellate cells (HSCs) become hyperactive and produce excessive ECM fibers. Furthermore, mechanical stimulation can encourage ECM secretion and remodeling of a fiber structure. Based on the above factors, we transfected HSCs with the hepatitis B viral X (*HBX*) gene for simulating the process of HBV infection. Subsequently, these *HBX*-HSCs were implanted into a polycaprolactone-polyurethane (PCL-PU) bilayer scaffold in which the inner layer is dense and the outer layer consists of pores, which was mechanically stimulated to promote the secretion of collagen nanofiber from the *HBX*-HSCs and to facilitate crosslinking with the scaffold. We obtained an ECM-PCL-PU composite bionic blood vessel that could act as access for dialysis after decellularization. Then, the vessel scaffold was implanted into a rabbit's neck arteriovenous fistula model. It exhibited strong tensile strength and smooth blood flow and formed autologous blood vessels in the rabbit's body. Our study demonstrates the use of human cells to create biomimetic dialysis blood vessels, providing a novel approach for creating clinical vascular access for dialysis.

Key words: Composite bilayer bionic blood vessel; Extracellular matrix (ECM); Hepatic stellate cells (HSCs); Hepatitis B viral X (*HBX*) gene; Mechanical force

1 Introduction

Hemodialysis treatment is administered annually to nearly three million patients who suffer from kidney failure around the world (Nesrallah et al., 2013). Autologous arteriovenous fistula (AVF) is the optimal choice for patients undergoing maintenance hemodialysis due to its exceptional histocompatibility and lack of immune rejection. When an autologous AVF is impossible, an artificial vascular graft (AVG) fistula is a feasible alternative (Gokal, 2002). There are numerous patients using AVG access for hemodialysis (Yang et al., 2013; Tang et al., 2022). Nonetheless, this approach still has critical issues that may require immediate attention (Stegemann et al., 2007; Fan et al., 2012). For instance, the elasticity and softness of artificial vessels differ greatly from those of human arteries,

✉ Yuanyuan ZHOU, 15959223830@163.com
Yilin ZHAO, zyllbz@gmail.com
* The two authors contributed equally to this work
Hongyi LIU, https://orcid.org/0000-0002-6005-6511
Yuanyuan ZHOU, https://orcid.org/0000-0002-0691-954X
Yilin ZHAO, https://orcid.org/0000-0003-2981-1803

Received July 10, 2023; Revision accepted Aug. 23, 2023; Crosschecked Apr. 10, 2024; Published online June 1, 2024

and the need for multiple punctures during vessel anastomosis and subsequent dialysis treatments may cause damage to the vascular scaffold, thus presenting significant challenges in matching AVG to anastomosed vessels compared to AVF. Failure to achieve this often leads to stenosis, thrombosis, and high infection rates (Bachleda et al., 2012).

The structure of natural blood vessels primarily consists of three layers: (1) the dense and smooth basement membrane that is rich in type IV collagen; (2) the middle layer composed of type I and type III collagens and elastin; and (3) the rough and porous outer layer containing randomly arranged type I collagen (Rhodes and Simons, 2007; Zhao et al., 2010; Wang et al., 2012; Mongiat et al., 2016; Zhou et al., 2018; Steffensen et al., 2021). Collagen contributes to the tensile strength of the vessel wall, while elastin provides elasticity (Wang et al., 2006). Therefore, collagen is the primary component in the extracellular matrix (ECM) that upholds the structure and mechanical characteristics of biological blood vessels (Cheng et al., 2009; Lu et al., 2021). On the one hand, although heterologous ECM is readily available, it poses potential risks of inter-species antigenicity. On the other hand, homologous ECM is antigen-free but is difficult to obtain for clinical use (Farb et al., 2004; Barberio et al., 2022). To circumvent these issues, it could be a promising approach to produce human-derived vascular ECM through the in vitro cultivation of human cells and thus avoid obtaining materials from living or deceased bodies. Therefore, researchers are exploring ways to create composite bionic blood vessels using human-derived ECM (Thottappillil and Nair, 2015).

A crucial aim of research in this field is to find a cell capable of robust proliferation and high human collagen secretion. Some studies have suggested that hepatic stellate cells (HSCs) are typically in a quiescent state under normal conditions (Bataller and Brenner, 2005; Seo et al., 2019; Batudeligen et al., 2023). However, in patients with hepatitis B virus (HBV), liver fibrosis occurs due to the continuous activation of HSCs by HBV, which leads to the excessive secretion of collagens and other ECM molecules (Bataller and Brenner, 2005; Martín-Vílchez et al., 2008; Khomich et al., 2019; Deng et al., 2021). In fibrosis, ECM accumulates abnormally and leads to a 3–5-fold increase in deposition compared to healthy livers (Bedossa and Paradis, 2003; Sánchez-Romero et al., 2019). HSCs have been identified as a potential source of human collagen production in vitro (Bataller and Brenner, 2005; Koyama and Brenner, 2017; Yin et al., 2023). Therefore, we can take advantage of the stimulatory effect of HBV on HSCs to produce large amounts of ECM. HBV consists of four open reading frames, one of which being the X region that encodes the hepatitis B viral X (HBX) protein. Several studies have shown that HBX activates hematopoietic stem cells by upregulating transforming growth factor β1 (TGFβ1) expression (Chen et al., 2014; Deng et al., 2021) and promotes liver fibrosis and hepatocarcinogenesis by downregulating microRNA (miR)-30e/miR-27a targeting prolyl 4-hydroxylase subunit α2 (*P4HA2*) messenger RNA (mRNA) (Feng et al., 2017; Zhang et al., 2018; Yang et al., 2021). Meanwhile, studies on the fabrication of tissue-engineered blood vessels have been scarce. In addition, it has been shown that mechanical stimulation increases ECM secretion and fiber structure formation (Sehgal et al., 1995; Daley and Yamada, 2013). Besides, the effect of combined biological and physical stimuli on HSC-LX2 secretion of the ECM has not been investigated. Thus, we utilized the stable transfection of a cell line of HSCs (HSC-LX2) with *HBX* to replicate the process of HBV infection and to enhance their ability to secrete ECM fibers, such as collagen fibers.

We developed a bionic blood vessel for dialysis by implanting the *HBX*-HSCs into a polycaprolactone-polyurethane (PCL-PU) bilayer scaffold in which the inner layer is dense and the outer layer is porous, which promotes the secretion of ordered collagen fibers by mechanical stimulation and facilitates cross-linking with the porous scaffold. Finally, we evaluated the therapeutic effect of this bionic blood vessel by implanting it into a rabbit's neck AVF model.

2 Materials and methods

2.1 Cell line development and evaluation

HSCs (HSC-LX2) and hepatocellular carcinoma cells with HBV infectivity (HepG2.2.15) were cultured in Dulbecco's modified Eagle medium (DMEM; Thermo Fisher, Waltham, Massachusetts, USA) supplemented with 10% (volume fraction) fetal bovine serum (FBS). Both cell lines were supplemented with penicillin (100 U/mL, Thermo Fisher) and streptomycin (100 μg/mL, Thermo Fisher) and maintained at 37 ℃ in a humidified atmosphere with 5% CO_2.

HBV indirectly infects LX2 cells (HBV-LX2). HepG2.2.15 was co-cultured with LX2 cells (LX2 and HepG2.2.15, Procell Life Science & Technology Ltd., Wuhan, China) in a transwell system at a quantitative ratio of 4:1, and HepG2.2.15 was cultured in a small chamber where its secreted HBX protein factor indirectly stimulated LX2 cells (Wang et al., 2016).

LX2 was stably transfected with *HBX* (*HBX*-LX2). The construction of the vector was outsourced to Shanghai Genechem Co., Ltd. (Shanghai, China). Plasmids were cultured and extracted by DH5α receptor cells (Biomed, Beijing, China) and the EndoFree Plasmid Midi Kit (Jiangsu Cowin Biotech Co., Ltd., Taizhou, China). Transfection was carried out using the Hieff Trans™ liposomal transfection reagent (Yeasen Biotechnology Co., Ltd., Shanghai, China), and the stable transfectant was selected using genomycin G418 (Li et al., 2011; Niu et al., 2022). The efficiency of transfection was corroborated by the HBX Quantitative Assay Kit (Huangshi Inselisa Biotechnology Co., Ltd., Huangshi, China).

Mechanical force dynamic cultivation: the cells (0, 100, and 200 r/min) or the scaffolds with cells (200 r/min) were fixed in a 6/12/24-well plate in the incubator (37 °C, 5% CO_2) to generate a laminar flow that simulates the effect of blood flow on cells; different mechanical forces were simulated through a mechanical shaker that vibrates in a circular pattern at different speeds.

2.2 Preparation and characterization of bilayer PCL-PU composite vascular scaffolds

2.2.1 Preparation of dense inner layer

PU was dissolved in solvent (*N*,*N*-dimethyl formamide: tetrahydrofuran=4:1 (volume ratio)) to 10% (volume fraction), and then sodium heparin was added as anticoagulant to prepare the PU fiber layer by electrospinning (Jirofti et al., 2018), with the following parameters: voltage, −10 and 20 kV; speed, 0.1 mL/h; diameter of the vessel receiver, 2 mm; rotation speed of the vessel receiver, 100 r/min; temperature, (25±2) °C; humidity, (50±5)%.

2.2.2 Preparation of porous outer layer

PCL was dissolved in dichloromethane at 5.9% (0.059 g/mL), and then NaCl 10% (0.1 g/mL) and (*Z*)-mono-9-octadecenoic acid-dehydrated sorbitan ester (Span-80) 1.5% (0.015 g/mL) were added to the PCL solution under stirring, which was continued with foaming for 1 h (Baker et al., 2009). This was coated on the outer surface of PU fiber layer, rapidly frozen and shaped at −80 °C for 12 h and freeze-dried by vacuum for 24 h. Finally, deionized water was used to remove NaCl and Span-80 by soaking to obtain a bilayer vascular scaffold with a dense inner layer and a porous outer layer. The fiber diameters of dense inner layer and pore sizes of porous outer layer were quantified by scanning electron microscopy (SEM) and FIJI software (Schindelin et al., 2012) and counted by Origin software.

2.2.3 Characterization of PCL-PU bilayer scaffolds

The material was soaked in phosphate-buffered saline (PBS) solution for 24 h, removed, weighed, and compared with the original weight to show the water absorption property (R_s). The calculation formula is:

$$R_s = (W_s - W_d)/W_d \times 100\%, \quad (1)$$

where R_s is the water absorption rate, W_s is the weight after immersion in PBS, and W_d is the original weight.

The porosity of PU dense layer was detected by Brunner-Emmet-Teller (BET) measurements (Micromeritics, USA, ASAP2020). The porosity of the PCL porous outer layer was measured by the squeezing method. The calculation formula (Zhao et al., 2010) is:

$$P = (1 - V/V_0) \times 100\%, \quad (2)$$

where P is the porosity, V_0 is the volume of the material in its natural state of different sizes, and V is the volume of the material in its extruded state of different sizes.

The cytotoxicity of PCL-PU was tested by cell counting kit-8 (CCK-8) assay and the cytocompatibility was assessed by SEM. In addition, sterilized PCL-PU vascular scaffolds were implanted into mice. The material and surrounding tissues were removed after 1, 2, and 6 weeks, and then their histocompatibility was assessed by hematoxylin and eosin (H&E) staining (Solarbio, Beijing, China).

2.3 Preparation and characterization of human-derived ECM-PCL-PU composite bionic blood vessels

HBX-LX2 cells (1×10^8 cells/cm^2) were seeded onto PCL-PU vascular scaffolds in six-well plates. After the cells had fully adhered and proliferated on the

scaffolds for 4 h, a complete medium was added to each well at an amount just enough to cover the scaffold material. The plate was then placed on a shaker and incubated at 200 r/min for dynamic culture. Subsequently, the composite scaffolds were removed from the plates and decellularized based on our previously published work (Zhao et al., 2010; Wang et al., 2012). This was achieved by treating the material with 0.25% (2.5 g/L) trypsin for 2–3 h, and RNA enzyme (1 unit RNA enzyme equivalent to 1 μg RNA) and DNA enzyme (1 unit DNA enzyme equivalent to 0.5 μg DNA) sequentially for 6 h, enabling the complete removal of cells with minimal breakage of the outer ECM. This resulted in the preparation of ECM-PCL-PU composite bio-vascular structure consisting of the ECM interwoven within the porous layer and on the surface of the dense layer.

The tensile properties of this vascular structure (10 mm) were tested using a WDW-100E Tensile Tester (Jinan Limai Hydraulic Pressure Co., Ltd., Jinan, China) by longitudinally stretching at 10 mm/min and recording the stress–strain curves and the maximum load and displacement (Do et al., 2021). The morphology and content of collagen fibers, elastic fibers, and reticular fibers (da Silva et al., 2017) were detected by Masson's Trichrome Stain Kit/van Gieson's Stain Kit, Victoria Blue Elastic Stain Kit, and Reticular Fiber Stain Kit (Solarbio), respectively.

The leakages of ECM-PCL-PU composite bionic blood vessels were tested by repeated puncture. After assembling and fixing a rubber tube with a peristaltic pump (Hebei, China), it was connected to the prepared ECM-PCL-PU composite bionic blood vessel to form a closed loop filled with distilled water. The peristaltic pump was turned on and the water was allowed to flow at the average blood flow rates of arteries (4.0 mL/s), veins (2.4 mL/s), and capillaries (3.2 mL/s). At the same time, the vessels were repeatedly punctured with a puncture needle until they leaked, and the number of needle sticks was recorded when the leakage occurred.

2.4 Quantification of ECM components

The cells obtained from dynamic cultivation were collected and subjected to detection of the presence of collagen, elastin, glycosaminoglycan (GAG), and hyaluronic acid (HA) using the ECM Detection Kit (Biocolor Ltd., UK) (Parry and Squire, 2005; Mecham, 2008; Stern, 2008; Schaefer and Schaefer, 2010; Sato et al., 2016).

2.5 Implantation of human-derived ECM-PCL-PU bionic blood vessels

Ten New Zealand rabbits underwent surgery to create vascular access models under general anesthesia. Artificial vessels were implanted between the external jugular vein and the common carotid artery. An ECM-PCL-PU composite bionic blood vessel was implanted in the experimental group (five rabbits), while in the control group (five rabbits) a vascular scaffold was implanted. Prior to suturing, 2 mL of heparin (12 500 U) was intravenously administered to animals in both groups. Postoperatively, the rabbits were given intramuscular injections of sodium penicillin to prevent infection. After six weeks, the rabbits were observed, sampled, and tested. Doppler ultrasound was used to observe the typical development of the AVF.

2.6 Statistical analysis

The experiment was performed in triplicate and the data were analyzed using GraphPad Prism 9.4.1 software. The results were presented as mean±standard error of the mean. Statistical significance was determined using two-way and one-way analyses of variance (ANOVA) followed by multiple comparisons. A P-value of less than 0.05 was considered statistically significant.

3 Results and discussion

3.1 Cell line development and evaluation

We employed two methods to activate LX2 cells: HBV-indirect infection (HBV-LX2) and *HBX* transfection (*HBX*-LX2) (Fig. 1a). The cell numbers were counted by a Fuchs-Rosenthal Counting Chamber (Hausser Scientific, USA) (Fig. 1b), which showed that the proliferation rate of activated LX2 cells was significantly higher than that of normal cells in the control group. These activated LX2 cells are responsible for producing ECMs. However, these ECM proteins exist in a disordered state, and further shaping is necessary to enhance their stiffness, including softness, toughness, strength, etc.

Mechanical shaker-induced dynamic cultivation inhibited cell proliferation, and the higher the rotational

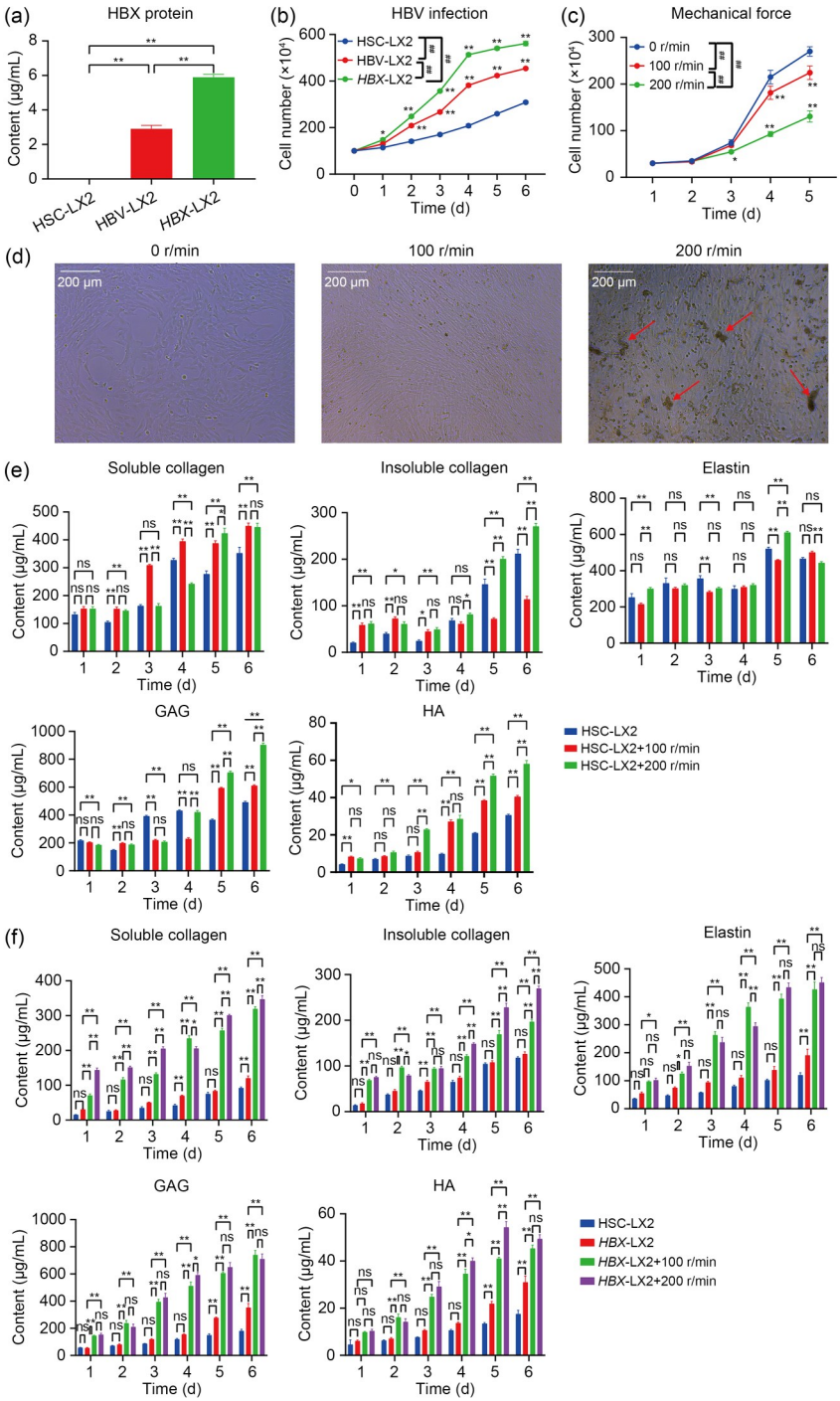

Fig. 1 Culture, processing, and assay of hepatic stellate cells. (a) Quantification of hepatitis B viral X (HBX) protein expression in LX2, hepatitis B virus (HBV)-LX2, and *HBX*-LX2 cells. (b, c) Effects of HBV infection (b) and mechanical force (c) on the proliferation of LX2 cells. $^{*}P$<0.05 and $^{**}P$<0.01, compared with LX2 or 0 r/min at the same time; $^{\#\#}P$<0.01, compared between different HBV infections or mechanical forces. (d) Effect of mechanical force stimulation on the morphology and growth of LX2 cells in a six-well plate observed under a light microscope. (e) Effect of mechanical force on extracellular matrix (ECM) secretion by LX2 cells. (f) Effect of *HBX* and mechanical force co-stimulation on ECM secretion by LX2 cells. Data are presented as mean±standard error of the mean (n=3) and were analyzed by Tukey's multiple comparisons test. ns: no significant difference; $^{*}P$<0.05, $^{**}P$<0.01. HSC-LX2: hepatic stellate cells; *HBX*-LX2: stable *HBX*-transfected HSC cells; HBV-LX2: LX2 cells indirectly infected with HBV; GAG: glycosaminoglycan; HA: hyaluronic acid.

speed of the shaker, the slower the cell proliferation (Fig. 1c). Meanwhile, we observed the cell morphology under a light microscope, and found that the cells grew with the direction of mechanical force, and at 200 r/min, some suspended cells could be observed (Fig. 1d, the red arrow). We further investigated the influence of mechanical force on the secretion of ECM by LX2, and both intensities of mechanical force (100 and 200 r/min) stimulated the secretion of collagen, which increased progressively with incubation time at 200 r/min (Fig. 1e). The promotion of synthesis and secretion by high-intensity mechanical force (200 r/min) appeared to be more pronounced for the total collagen amount. The effect of mechanical force on the elastin content was minor, with a slight increase due to high-intensity mechanical force (200 r/min), which, in combination with cell proliferation results, increased significantly on the 5th and 6th days in the presence of reduced value-added rate. The mechanical force promoted the secretion of GAG, especially HA, and on the 5th and 6th days, their contents increased significantly under high-intensity mechanical force (200 r/min). Interestingly, although the mechanical force generated at 200 r/min inhibited the growth of cells, they produced more ECMs.

Furthermore, the combined effect of mechanical force and *HBX* transfection on ECM secretion was examined by applying different forces to HSC-LX2 and *HBX*-LX2 (Fig. 1f). *HBX* transfection was found to activate HSC-LX2 and secret various ECMs, such as collagen, elastin, and GAG, albeit with a limited effect. Meanwhile, the ECM was significantly increased when mechanical force was applied to *HBX*-LX2. Upon higher mechanical force (200 r/min), it could more effectively stimulate the secretion of ECM. When mechanical force was applied to *HBX*-LX2 cells, the inhibitory effect of mechanical force on proliferation was counteracted by the activating effect of *HBX*, and the promotive effect of both on ECM fiber secretion was superimposed. Therefore, we decided to use *HBX*-LX2 cells dynamically cultured at 200 r/min as the seed cells for vascular tissue engineering.

3.2 Preparation and characterization of PCL-PU bilayer vascular scaffolds

The PCL-PU bilayer vascular scaffold with dense inner layer and porous outer layer exhibited a soft and elastic surface, so that it could maintain its tubular structure without folding even when it was made into a U-shape (Fig. 2a). The outer diameter of the tube walls was measured as (2.00±0.33) mm and the thickness as (0.39±0.03) mm by Vernier caliper. The two layers were tested independently under SEM (Fig. 2b). The SEM images and pore diameters of the outer layer showed that the layer has small pores of varying sizes with a depth of 20−250 μm (Fig. 2c), and the porosity was calculated to be (78.01±1.80)% according to Eq. (2) (Table 1). The SEM images of the inner layer and fiber diameter distribution showed dense fiber distribution, the adsorption average pore width was 2 nm, the layers were interlaced, and the filaments were nanoscale (Fig. 2d).

We then conducted an assessment of the PCL-PU scaffold and found that it exhibited excellent hydrophilicity, with the ability to absorb liquid more than twice its weight, reaching 255.18% (Fig. 2e). For LX2 cells with a complete medium with 200 μg/mL PCL-PU as the testing group, we observed no discernible difference in proliferation rates between the experimental and control groups (Fig. 2f). Additionally, the material exhibited good cell compatibility, with LX2 cells being able to adhere, grow, and proliferate normally when viewed under SEM (Fig. 2g). We discovered that the porous structure of PCL-foaming layer was ideal for cell adhesion. Furthermore, the scaffold demonstrated good tissue compatibility, as the sterilized material was gradually absorbed by the body and fully integrated after six months (Fig. 2h). Therefore, the PCL-PU scaffold we prepared was suitable for the in vitro preparation of ECM fiber-rich tissue-engineered vessels.

3.3 Preparation and detection of human-derived ECM-PCL-PU composite bionic blood vessels

We cultivated dynamic composite biomimetic blood vessels at 200 r/min and analyzed the ECM fiber content in the ECM-PCL-PU composite biomimetic blood vessels created by three different types of cells. We found that the contents of various ECMs were higher in the *HBX*-LX2 cell group than in the HSC-LX2 and HBV-LX2 groups. In these cells, the levels of ECMs, such as collagen and elastin secreted by *HBX*-LX2, were relatively high, reaching a peak at the 2nd week and showing little change from the 2nd to 4th weeks (Fig. 3a). Therefore, we chose *HBX*-LX2 cells to manufacture ECM-PCL-PU composite biomimetic blood vessels and analyzed the characteristics of these vessels.

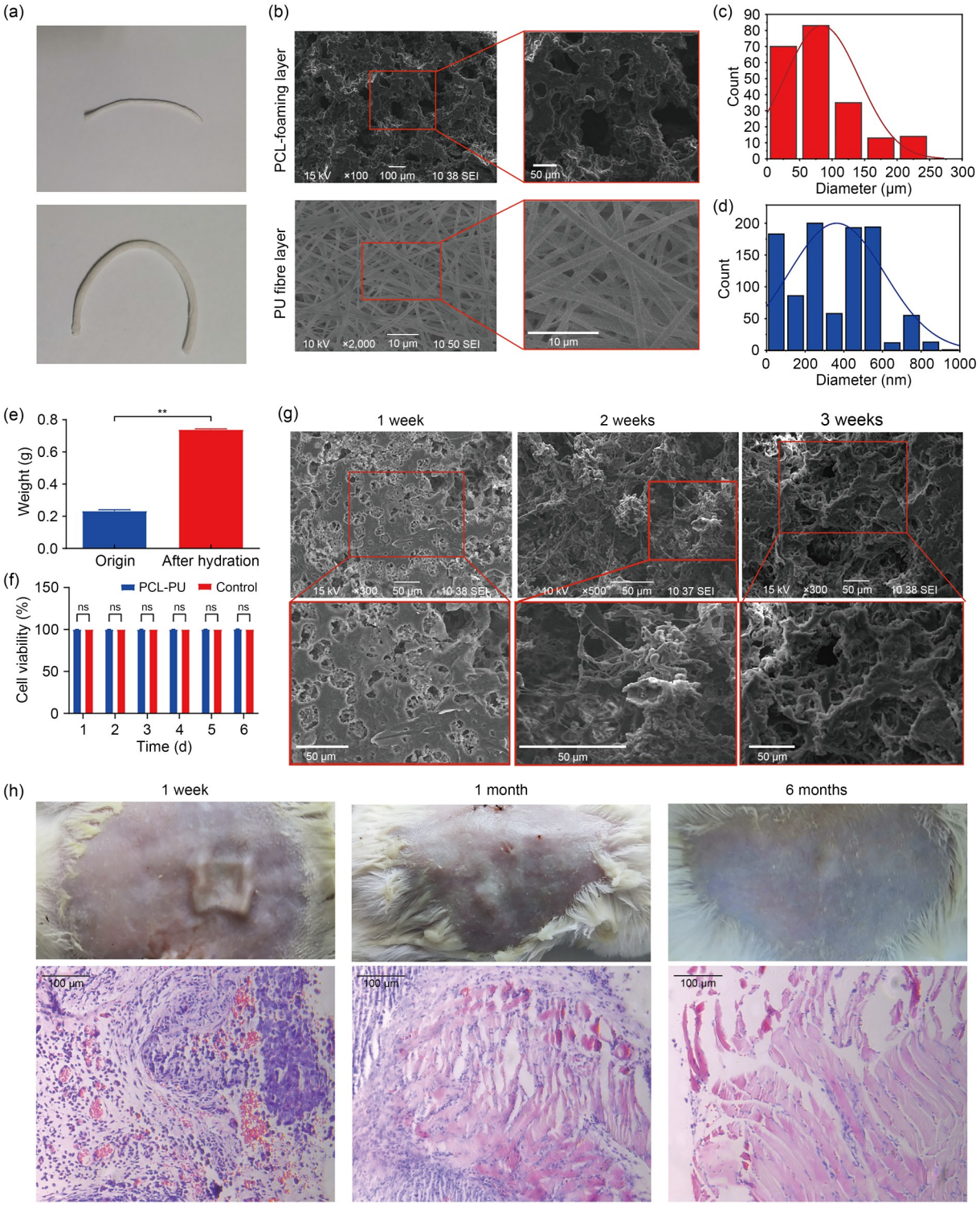

Fig. 2 Preparation and testing of polycaprolactone-polyurethane (PCL-PU) composite bio-vascular scaffolds. (a) The surface of the vascular scaffold is soft. Bending into a U-shape can still maintain the tubular structure without fracture, and smooth flow remains in the lumens. (b) Scanning electron microscopy (SEM) images of a PCL-PU vascular scaffold: the structure of the PCL-foaming layer and the structure of the PU fiber layer. (c) Pore distribution of the porous outer layer. (d) Fiber diameter distribution of the dense inner layer. (e) Hydrophilicity. (f) Cytotoxicity assay. (g) Cytocompatibility testing. (h) Histocompatibility testing. The data in (e) and (f) are presented as mean±standard error of the mean (n=3) and were analyzed by Tukey's multiple comparisons test. ns: no significant difference; $^{**}P$<0.01.

Table 1 Porosity testing of polycaprolactone-polyurethane (PCL-PU) bilayer vascular scaffolds

No.	Length (mm)	Width (mm)	Thickness (mm)	V_0 (mm^3)	V (mm^3)	P (%)
1	11.52	10.58	0.21	25.60	5.78	77.42
2	10.22	11.20	0.24	27.47	6.05	77.98
3	11.42	10.70	0.20	24.44	5.99	75.49
4	11.15	10.61	0.22	26.03	6.44	75.26
5	10.98	11.78	0.19	24.58	5.27	78.56
6	10.62	11.24	0.24	28.65	6.39	77.70
7	10.47	10.56	0.24	26.54	5.15	80.59
8	11.38	11.09	0.23	29.03	5.66	80.50
9	10.78	11.56	0.22	27.42	6.24	77.24
10	10.67	10.56	0.22	24.79	5.21	78.98
Average	10.92	10.99	0.22	26.45	5.82	78.01

V_0: the volume of the material in its natural state of different sizes; V: the volume of the material in its extruded state of different sizes; P: porosity.

The PCL-PU composite bionic vessels exhibited strong tensile strength (Figs. 3b, 3c, and 3g) and possessed stiffness and softness similar to decellularized natural vessels obtained from rabbit carotid arteries (Zhao et al., 2010; Zhou et al., 2018). When dynamically cultured for 2–3 weeks, ECM-PCL-PU possessed stronger stiffness and softness than the natural vessels, and after four weeks, their softness decreased, possibly accompanied by an ECM production-metabolism shift. In addition, cells cultured under certain direction of force grew and secreted ECM fibers along the direction of force, which was reflected in the results of stress–strain tests (Fig. 3g). Since ECM-PCL-PU composite bio-vessels are prepared as bilayers, they break twice during stretching, with the outer porous layer breaking first and the inner one breaking later. Moreover, they demonstrated excellent hydrophilicity (Fig. 3d), with a maximum absorption rate exceeding 300.00%. The maximum hydrophilicity and tensile strength occurred during the 2–3 weeks following the implantation of cells. Furthermore, the ECM-PCL-PU composite bionic blood vessels obtained with dynamic culture displayed significantly greater puncture resistance compared to the remaining two vessel groups in the repeated puncture tests and did not differ from natural rabbit carotid decellularized vessels (Fig. 3e). This indicated that their softness and tensile strength were similar to those of natural vessels because the PU fiber layer had a dense and compressed structure, providing elastic support and repeated puncture function for the vascular scaffold. SEM revealed cell growth and the ordered secretion of ECM fibers, and observed the structure of cells and the ECM after cell seeding, adherence, proliferation, and decellularization (Zhao et al., 2010; Wang et al., 2012) (Fig. 3h). The DNA content detected in ECM-PCL-PU demonstrated that decellularization had been thoroughly accomplished ((0.060± 0.004) ng/mg dry weight) (Fig. 3f). Over time, cell growth on PCL-PU scaffolds was clearly visible through H&E staining. Various staining techniques, including Masson's trichrome/van Gieson, elastic fiber, and reticular fiber stainings, were used to identify different components of the ECMs, such as collagen fibers, elastic fibers, and reticular fibers, respectively (Fig. 3i). Therefore, we conducted a 2–3-week dynamic culture (PCL-PU+*HBX*-LX2+mechanical force) of *HBX*-LX2 cells on a PCL-PU scaffold to prepare a biomimetic blood vessel.

The ECM functions within a complex mechanical framework in which various components are regulated by mechanical forces. These components possess the capability of translating mechanical cues into corresponding biochemical responses (Wang and Thampatty, 2006; Peyton et al., 2007). The transmembrane protein integrin functions as a mechanical shaker-induced dynamic cultivation by being externally linked to collagen by fibronectin and internally connected to the actin backbone through an adhesive patch structure, which results in the development of a complete mechanical conduction pathway (Huang et al., 2006; Kechagia et al., 2019). Mechanical force plays an integral role in the behavior of cells. It not only encourages the secretion of ECM but also facilitates the cross-linking of collagen in multiple directions. In this work, the high-frequency circular motion of the shaker promoted the longitudinal growth of cells along the direction of the force in the vascular scaffold. This resulted in the production of ECM fibers that are cross-linked with the scaffold, making them more suitable for blood flow within the vessel. The product was a composite bionic blood vessel with high hydrophilicity, exceptional tensile strength, and strong elastic recovery force. The elastic recovery force was especially evident in the puncture process, in which the needle created a pathway without damaging the structure of blood vessel wall. When the dialysis needle was inserted and removed, biological tissue quickly regained its shape, leading to fast hemostasis.

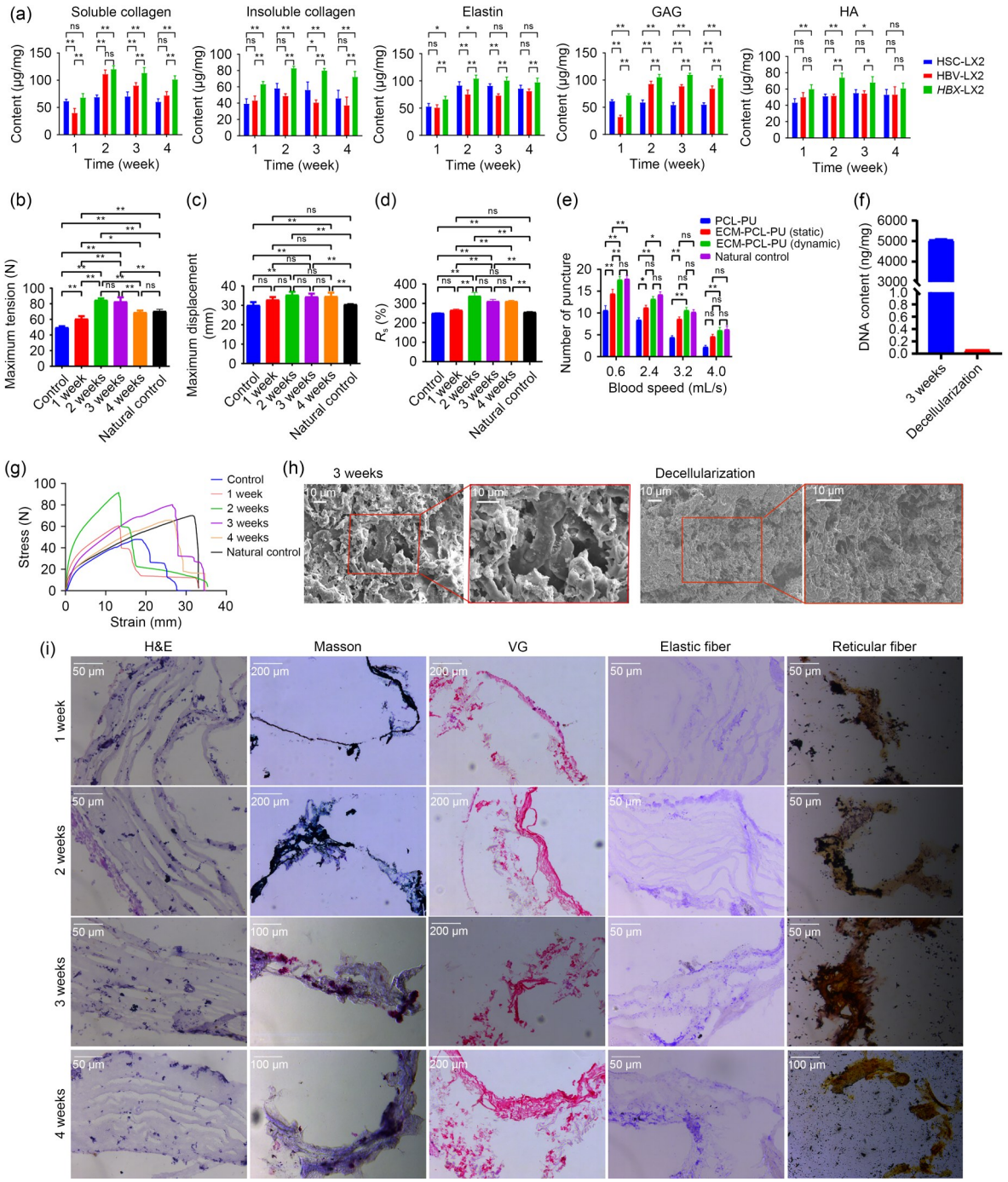

Fig. 3 Preparation and characterization of human-derived extracellular matrix-polycaprolactone-polyurethane (ECM-PCL-PU) composite bilayer bionic blood vessels. (a) Quantitative ECM analysis of human-derived ECM-PCL-PU composite vessels at 200 r/min. (b, c) Tensile force test: maximum tension (b) and maximum displacement (c). (d) Water absorption rate (R_s) test (hydrophilicity). (e) Repeated puncture test. (f) DNA content of ECM-PCL-PU. (g) Stress–strain curve. (h) Scanning electron microscopy (SEM) showed that the growth of *HBX*-LX2 cells covered the surface of the scaffold after three weeks and large amounts of ECMs were retained after decellularization. (i) Hematoxylin and eosin (H&E) staining, Masson's trichrome staining (collagen is blue), van Gieson (VG) staining (collagen is red), elastic fiber staining (elastic fiber is blue), and reticular fiber staining (reticular fibers are black and collagen is yellow) to evaluate the cell growth and ECM secretion on the surface of artificial blood vessels. Data in (a–f) are presented as mean±standard error of the mean (n=3) and were analyzed by Tukey's multiple comparisons test. ns: no significant difference; $^{*}P$<0.05, $^{**}P$<0.01. GAG: glycosaminoglycan; HA: hyaluronic acid.

3.4 Bio-vascularization of rabbit neck graft using a composite of human-derived ECM-PCL-PU

After constructing the vascular access model (Fig. 4a), we used Doppler ultrasound inspection to scan the neck vessels of rabbits at the 1st, 2nd, and 4th weeks. Our results showed that the ECM-PCL-PU bionic blood vessels in the experimental group had superior inner diameter, area, and blood flow velocity compared to the PCL-PU scaffolds in the control group. At the 4th week, we found that all bionic blood vessels in the experimental group remained patent, while the scaffolds in the control group were occluded (Fig. 4b).

In order to observe the formation of collateral circulation around the trans-planted vessels, we incised the right neck of the rabbits (Fig. 4c). In the control group, the boundary between the vessels and surrounding tissues was blurry. In contrast, the boundary was clear in the experimental group, and the integration with normal rabbit tissues was better. We then removed the artificial vessels by stripping them from the surrounding tissues and analyzed their cross-sections. We found that most of the vessels in the control group were occluded with visible white transparent thrombus (Fig. 4c, at the red arrow). Meanwhile, the vessels in the experimental group remained intact, with mostly patent lumens and a smooth inner surface. H&E staining revealed that the control of vascular scaffolds had thin walls, small luminal inner diameter, and sparse cell arrangement. The composite bionic blood vessels in the treated group had thick walls with obvious hyperplasia and tightly arranged cells (Fig. 4d). We then used SEM to observe the luminal surface of the artificial vessel. The cellular coverage of the lumen surface of ECM-PCL-PU composite vessels was higher than that of PCL-PU (Fig. 4e), and the porous layer of ECM-PCL-PU vessels fused better with cells in vivo than that of PCL-PU, which was more favorable for maintaining the degradation of ECM-PCL-PU vascular material and autologous angiogenesis simultaneously, whereas the rate of the degradation of PCL-PU was greater than that of the autologous angiogenesis, with the emergence of more fine voids on the surface. Eventually, it could produce circulating blood vessels that belonged entirely to the body itself.

Additional testing was performed to evaluate the efficacy of the transplanted blood vessels. The results of tensile testing indicated no significant changes in the maximum displacement of the PCL-PU scaffolds after implantation, while the ECM-PCL-PU vessels showed a notable increase in maximum displacement. Both groups exhibited an increase in the maximum load (Fig. 4f). To assess the inflammatory response, enzyme-linked immunosorbent assay (ELISA) was performed on samples of synthetic vascular material after implantation, revealing lower levels of the inflammatory cytokine (Rose-John et al., 2015) interleukin (IL)-6 in the ECM-PCL-PU group compared to the PCL-PU group. In addition, the ECM-PCL-PU group exhibited higher levels of the anti-inflammatory factor (Kim et al., 2023) IL-10 (Fig. 4g). Therefore, we concluded that PCL-PU scaffolds were more susceptible to inflammation reactions compared to ECM-PCL-PU bionic blood vessels when implanted into rabbits.

Furthermore, it was evident that the ECM-PCL-PU bionic blood vessels implanted into the rabbits newly produced more collagen and elastin proteins than the PCL-PU scaffolds by ECM assay kits. However, there was no significant difference in the production of GAG or HA between the two groups (Fig. 4h). We were pleasantly surprised to find that the initial ECM content would affect the host cell tensor and ECM production after implantation. Therefore, ECM-PCL-PU bilayer bionic vessels were more likely to fuse with surrounding tissues and form autologous tissues in rabbits.

Due to their excellent hydrophilicity and inner layer compactness, PCL-PU scaffolds had excellent sutures and could absorb extensive amounts of heparin solution and maintain smooth blood flow after implantation into rabbits without clotting. However, when the heparin levels depleted, PCL-PU scaffolds struggled to integrate with the surrounding tissues of rabbits and form autologous blood vessels in a short amount of time, which increased the risk of clotting. Conversely, ECM-PCL-PU composite bionic blood vessels offered a unique solution. When implanted into the neck of rabbits, they could effectively form autologous blood vessels, prevent inflammatory reactions, and guarantee smooth blood flow. Some rabbits might even experience heart failure due to excessive smoothness. ECM-PCL-PU bionic blood vessels could fuse with surrounding tissue cells, promote continuous growth, and increase the content of ECM, such as collagen and elastin. As the PCL-PU scaffold material degraded, it was replaced by the rabbit's own tissue. Therefore, ECM materials could not only improve the stiffness of artificial blood vessels but also promote the metabolic process.

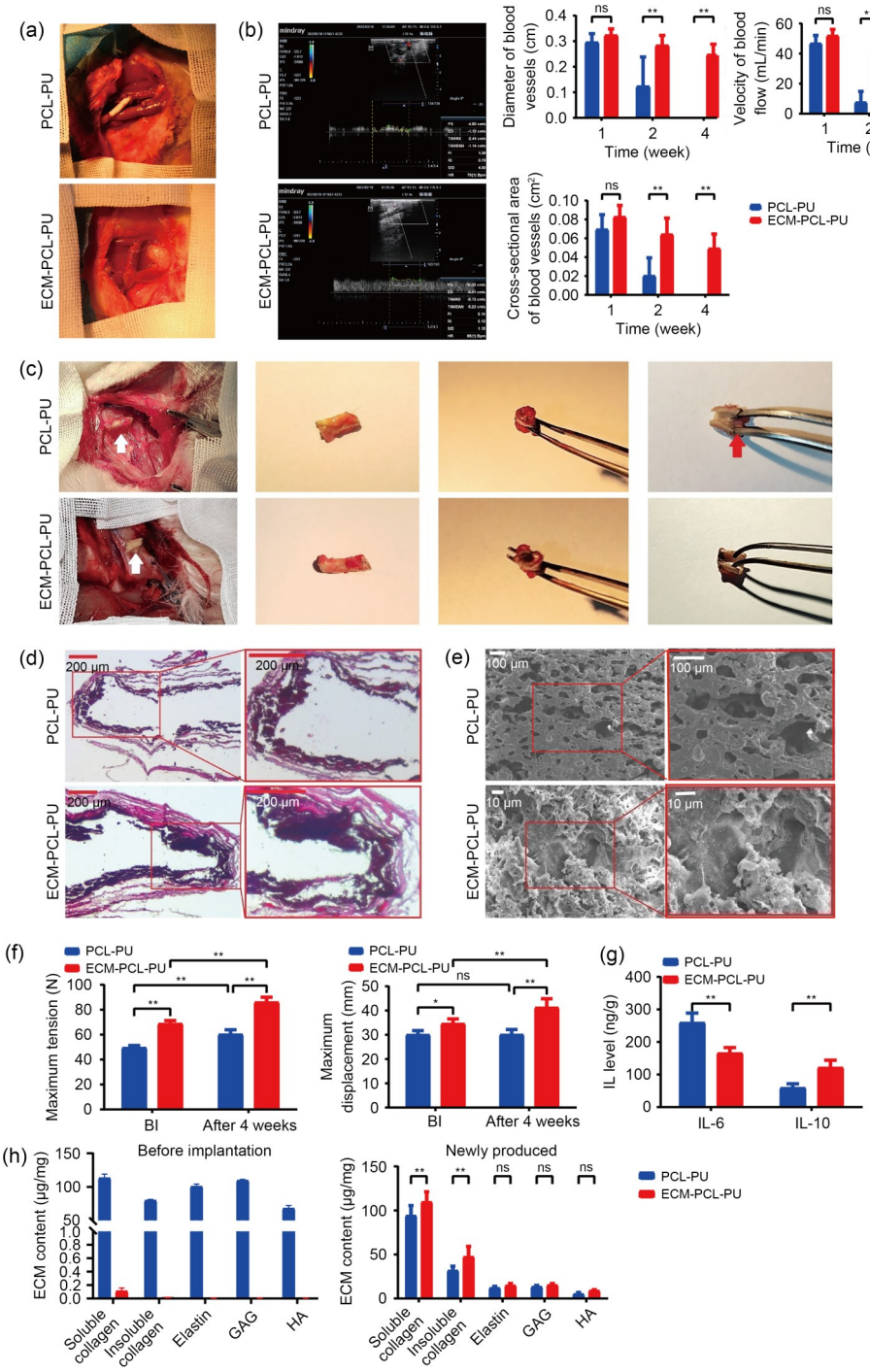

Fig. 4 Human-derived extracellular matrix-polycaprolactone-polyurethane (ECM-PCL-PU) composite bio-vascular graft. (a) Implantation of artificial blood vessels in the neck of rabbits. (b) Statistics of vessel diameter, area, and blood flow velocity by color Doppler ultrasound. (c) Results of neck incisional exploration. The white arrows point to the successful junction of the PCL-PU/ECM-PCL-PU vascular scaffolds. The red arrow shows the inner layer where newly produced fibers from the rabbit itself merge with the material. (d) Cross-sectional morphology of artificial blood vessels investigated by hematoxylin and eosin (H&E) staining. (e) Artificial blood vessel intima observed by scanning electron microscopy (SEM). (f) Tensile force testing of artificial blood vessels. (g) Enzyme-linked immunosorbent assay (ELISA) for interleukins (ILs), IL-6 as a pro-inflammatory factor and IL-10 as an anti-inflammatory factor. (h) Detection of regeneration in the ECM of artificial blood vessels. Data are presented as mean±standard error of the mean (n=3) and were analyzed by Tukey's multiple comparisons test. ns: no significant difference; $^{*}P$<0.05, $^{**}P$<0.01. GAG: glycosaminoglycan; HA: hyaluronic acid; BI: before implantation.

4 Conclusions

In summary, we constructed a novel artificial blood vessel model for dialysis that features large numbers of ECM fibers. Firstly, inspired by the fibrotic effects of HBV infection, we prepared cells secreting large amounts of ECMs, especially collagen. Secondly, we fabricated bilayer vascular scaffolds (PCL-PU) suitable for cell growth and adhesion, which contained large amounts of ordered ECM fibers (ECM-PCL-PU) under co-culture of *HBX*-LX2 and mechanical forces. Finally, the excellent performance of ECM-PCL-PU was demonstrated in an experimental model of rabbit carotid artery graft. We found that the initial ECM content would affect the production of ECM after implantation. Our findings form a basis to produce standardized processes, with the potential to overcome the limitations of artificial vessels currently used for clinical dialysis.

Data availability statement

The authors declare that the experimental data supporting the findings of this study are available within the paper.

Acknowledgments

This work was supported by the National Natural Science Foundation of China (No. 81770294) and the Natural Science Foundation of Fujian Province (No. 2023J05261), China.

Author contributions

Hongyi LIU carried out animal and cell experiments such as stable *HBX*-transfected HSCs and HBV-indirect infection, and drew images. Yuanyuan ZHOU completed the preparation of artificial vascular scaffolds such as PCL-PU and ECM-PCL-PU, and performed the characterization of artificial vascular materials such as tensile properties, special staining, and the detection of ECM content. Hongyi LIU and Yuanyuan ZHOU analyzed the results of all experiments, and wrote and edited the manuscript together. Peng GUO, Xiongwei ZHENG, Weibin CHEN, Shichao ZHANG, and Yu FU carried out cellular experiments. Xu ZHOU, Zheng WAN, and Bin ZHAO worked as an assistant in animal experiments. Yilin ZHAO conceived the design, analyzed the results, directed the experimental direction, and funded the study. All authors have read and approved the final manuscript, and therefore, have full access to all the data in the study and take responsibility for the integrity and security of the data.

Compliance with ethics guidelines

Hongyi LIU, Yuanyuan ZHOU, Peng GUO, Xiongwei ZHENG, Weibin CHEN, Shichao ZHANG, Yu FU, Xu ZHOU, Zheng WAN, Bin ZHAO, and Yilin ZHAO declare that they have no conflict of interest.

All institutional and national guidelines for the care and use of laboratory animals were followed (Xiamen University Laboratory Animal Center: Ethics No. XMULAC20170005).

References

Bachleda P, Kalinova L, Utikal P, et al., 2012. Infected prosthetic dialysis arteriovenous grafts: a single dialysis center study. *Surg Infect (Larchmt)*, 13(6):366-370. https://doi.org/10.1089/sur.2011.041

Baker SC, Rohman G, Southgate J, et al., 2009. The relationship between the mechanical properties and cell behaviour on PLGA and PCL scaffolds for bladder tissue engineering. *Biomaterials*, 30(7):1321-1328. https://doi.org/10.1016/j.biomaterials.2008.11.033

Barberio C, Saez J, Withers A, et al., 2022. Conducting polymer-ECM scaffolds for human neuronal cell differentiation. *Adv Healthc Mater*, 11(20):2200941. https://doi.org/10.1002/adhm.202200941

Bataller R, Brenner DA, 2005. Liver fibrosis. *J Clin Invest*, 115(2):209-218. https://doi.org/10.1172/JCI24282

Batudeligen, Han ZQ, Chen HM, et al., 2023. Luteolin alleviates liver fibrosis in rat hepatic stellate cell HSC-T6: a proteomic analysis. *Drug Des Devel Ther*, 17:1819-1829. https://doi.org/10.2147/DDDT.S402864

Bedossa P, Paradis V, 2003. Liver extracellular matrix in health and disease. *J Pathol*, 200(4):504-515. https://doi.org/10.1002/path.1397

Chen HY, Chen ZX, Huang RF, et al., 2014. Hepatitis B virus X protein activates human hepatic stellate cells through upregulating TGFβ1. *Genet Mol Res*, 13(4):8645-8656. https://doi.org/10.4238/2014.October.27.4

Cheng NC, Estes BT, Awad HA, et al., 2009. Chondrogenic differentiation of adipose-derived adult stem cells by a porous scaffold derived from native articular cartilage extracellular matrix. *Tissue Eng Part A*, 15(2):231-241. https://doi.org/10.1089/ten.tea.2008.0253

Daley WP, Yamada KM, 2013. ECM-modulated cellular dynamics as a driving force for tissue morphogenesis. *Curr Opin Genet Dev*, 23(4):408-414. https://doi.org/10.1016/j.gde.2013.05.005

da Silva WF, Simões MJ, Gutierre RC, et al., 2017. Special dyeing, histochemistry, immunohistochemistry and ultrastructure: a study of mast cells/eosinophilic granules cells (MCs/EGC) from *Centropomus parallelus* intestine. *Fish Shellfish Immunol*, 60:502-508. https://doi.org/10.1016/j.fsi.2016.11.022

Deng WY, Chen F, Zhou ZY, et al., 2021. Hepatitis B virus promotes hepatocellular carcinoma progression synergistically with hepatic stellate cells *via* facilitating the expression and secretion of ENPP2. *Front Mol Biosci*, 8:745990. https://doi.org/10.3389/fmolb.2021.745990

Do TD, Katsuyoshi J, Cai HN, et al., 2021. Mechanical properties of isolated primary cilia measured by micro-tensile

test and atomic force microscopy. *Front Bioeng Biotechnol*, 9:753805. https://doi.org/10.3389/fbioe.2021.753805

Fan WX, Deng ZX, Liu F, et al., 2012. Spontaneous retroperitoneal hemorrhage after hemodialysis involving anticoagulant agents. *J Zhejiang Univ-Sci B (Biomed & Biotechnol)*, 13(5):408-412. https://doi.org/10.1631/jzus.B1100357

Farb A, Kolodgie FD, Hwang JY, et al., 2004. Extracellular matrix changes in stented human coronary arteries. *Circulation*, 110(8):940-947. https://doi.org/10.1161/01.CIR.0000139337.56084.30

Feng GX, Li J, Yang Z, et al., 2017. Hepatitis B virus X protein promotes the development of liver fibrosis and hepatoma through downregulation of miR-30e targeting P4HA2 mRNA. *Oncogene*, 36(50):6895-6905. https://doi.org/10.1038/onc.2017.291

Gokal R, 2002. Peritoneal dialysis in the 21st century: an analysis of current problems and future developments. *J Am Soc Nephrol*, 13(Suppl 1):S104-S115. https://doi.org/10.1681/ASN.V13suppl_1s104

Huang JM, Tian XX, Zhong YF, et al., 2006. Effects of β1-integrin, fibronectin and laminin on invasive behavior of human gliomas. *Chin J Pathol*, 35(8):478-482 (in Chinese). https://doi.org/10.3760/j.issn:0529-5807.2006.08.007

Jirofti N, Mohebbi-Kalhori D, Samimi A, et al., 2018. Small-diameter vascular graft using co-electrospun composite PCL/PU nanofibers. *Biomed Mater*, 13(5):055014. https://doi.org/10.1088/1748-605X/aad4b5

Kechagia JZ, Ivaska J, Roca-Cusachs P, 2019. Integrins as biomechanical sensors of the microenvironment. *Nat Rev Mol Cell Biol*, 20(8):457-473. https://doi.org/10.1038/s41580-019-0134-2

Khomich O, Ivanov AV, Bartosch B, 2019. Metabolic hallmarks of hepatic stellate cells in liver fibrosis. *Cells*, 9(1):24. https://doi.org/10.3390/cells9010024

Kim SY, Park JH, Leite G, et al., 2023. Interleukin-10 knockout mice do not reliably exhibit macroscopic inflammation: a natural history endoscopic surveillance study. *Dig Dis Sci*, 68(5):1858-1862. https://doi.org/10.1007/s10620-023-07871-y

Koyama Y, Brenner DA, 2017. Liver inflammation and fibrosis. *J Clin Invest*, 127(1):55-64. https://doi.org/10.1172/JCI88881

Li W, Liu HY, Huang Z, 2011. Construction of luxAB-labelled *Pseudomonas aeruginosa*. *J Hyg Res*, 40(1):57-60 (in Chinese). https://doi.org/10.19813/j.cnki.weishengyanjiu.2011.01.012

Lu L, Shang XF, Liu B, et al., 2021. Repair of articular cartilage defect using adipose-derived stem cell-loaded scaffold derived from native cartilage extracellular matrix. *J Cell Physiol*, 236(6):4244-4257. https://doi.org/10.1002/jcp.30020

Martín-Vílchez S, Sanz-Cameno P, Rodríguez-Muñoz Y, et al., 2008. The hepatitis B virus X protein induces paracrine activation of human hepatic stellate cells. *Hepatology*, 47(6):1872-1883. https://doi.org/10.1002/hep.22265

Mecham RP, 2008. Methods in elastic tissue biology: elastin isolation and purification. *Methods*, 45(1):32-41. https://doi.org/10.1016/j.ymeth.2008.01.007

Mongiat M, Andreuzzi E, Tarticchio G, et al., 2016. Extracellular matrix, a hard player in angiogenesis. *Int J Mol Sci*, 17(11):1822. https://doi.org/10.3390/ijms17111822

Nesrallah GE, Mustafa RA, Macrae J, et al., 2013. Canadian society of nephrology guidelines for the management of patients with ESRD treated with intensive hemodialysis. *Am J Kidney Dis*, 62(1):187-198. https://doi.org/10.1053/j.ajkd.2013.02.351

Niu QY, Su XM, Lian LX, et al., 2022. Developing qualitative plasmid DNA reference materials to detect mechanisms of quinolone and fluoroquinolone resistance in foodborne pathogens. *Foods*, 11(2):154. https://doi.org/10.3390/foods11020154

Parry DAD, Squire JM, 2005. Fibrous proteins: new structural and functional aspects revealed. *Adv Protein Chem*, 70:1-10. https://doi.org/10.1016/S0065-3233(05)70001-2

Peyton SR, Ghajar CM, Khatiwala CB, et al., 2007. The emergence of ECM mechanics and cytoskeletal tension as important regulators of cell function. *Cell Biochem Biophys*, 47(2):300-320. https://doi.org/10.1007/s12013-007-0004-y

Rhodes JM, Simons M, 2007. The extracellular matrix and blood vessel formation: not just a scaffold. *J Cell Mol Med*, 11(2):176-205. https://doi.org/10.1111/j.1582-4934.2007.00031.x

Rose-John S, Scheller J, Schaper F, 2015. "Family reunion"—a structured view on the composition of the receptor complexes of interleukin-6-type and interleukin-12-type cytokines. *Cytokine Growth Factor Rev*, 26(5):471-474. https://doi.org/10.1016/j.cytogfr.2015.07.011

Sánchez-Romero N, Sainz-Arnal P, Pla-Palacín I, et al., 2019. The role of extracellular matrix on liver stem cell fate: a dynamic relationship in health and disease. *Differentiation*, 106:49-56. https://doi.org/10.1016/j.diff.2019.03.001

Sato N, Kohi S, Hirata K, et al., 2016. Role of hyaluronan in pancreatic cancer biology and therapy: once again in the spotlight. *Cancer Sci*, 107(5):569-575. https://doi.org/10.1111/cas.12913

Schaefer L, Schaefer RM, 2010. Proteoglycans: from structural compounds to signaling molecules. *Cell Tissue Res*, 339:237-246. https://doi.org/10.1007/s00441-009-0821-y

Schindelin J, Arganda-Carreras I, Frise E, et al., 2012. Fiji: an open-source platform for biological-image analysis. *Nat Methods*, 9(7):676-682. https://doi.org/10.1038/nmeth.2019

Sehgal PB, Wang L, Rayanade R, et al., 1995. Interleukin-6-type cytokines. *Ann N Y Acad Sci*, 762(1):1-14. https://doi.org/10.1111/j.1749-6632.1995.tb32309.x

Seo HY, Lee SH, Lee JH, et al., 2019. Clusterin attenuates hepatic fibrosis by inhibiting hepatic stellate cell activation and downregulating the Smad3 signaling pathway. *Cells*, 8(11):1442.

https://doi.org/10.3390/cells8111442

Steffensen LB, Stubbe J, Lindholt JS, et al., 2021. Basement membrane collagen IV deficiency promotes abdominal aortic aneurysm formation. *Sci Rep*, 11:12903. https://doi.org/10.1038/s41598-021-92303-y

Stegemann JP, Kaszuba SN, Rowe SL, 2007. Review: advances in vascular tissue engineering using protein-based biomaterials. *Tissue Eng*, 13(11):2601-2613. https://doi.org/10.1089/ten.2007.0196

Stern R, 2008. Hyaluronan in cancer biology. *Semin Cancer Biol*, 18(4):237. https://doi.org/10.1016/j.semcancer.2008.04.001

Tang XY, Chen DZ, Zhang L, et al., 2022. Application of regional citrate anticoagulation in patients at high risk of bleeding during intermittent hemodialysis: a prospective multicenter randomized controlled trial. *J Zhejiang Univ-Sci B (Biomed & Biotechnol)*, 23(11):931-942. https://doi.org/10.1631/jzus.B2200082

Thottappillil N, Nair PD, 2015. Scaffolds in vascular regeneration: current status. *Vasc Health Risk Manag*, 11:79-91. https://doi.org/10.2147/VHRM.S50536

Wang C, Garcia M, Lu X, et al., 2006. Three-dimensional mechanical properties of porcine coronary arteries: a validated two-layer model. *Am J Physiol Heart Circ Physiol*, 291(3): H1200-H1209. https://doi.org/10.1152/ajpheart.01323.2005

Wang J, Shen T, Huang XB, et al., 2016. Serum hepatitis B virus RNA is encapsidated pregenome RNA that may be associated with persistence of viral infection and rebound. *J Hepatol*, 65(4):700-710. https://doi.org/10.1016/j.jhep.2016.05.029

Wang JHC, Thampatty BP, 2006. An introductory review of cell mechanobiology. *Biomech Model Mechanobiol*, 5:1-16. https://doi.org/10.1007/s10237-005-0012-z

Wang JL, Cui WG, Ye JH, et al., 2012. A cellular delivery system fabricated with autologous BMSCs and collagen scaffold enhances angiogenesis and perfusion in ischemic hind limb. *J Biomed Mater Res A*, 100A(6):1438-1447. https://doi.org/10.1002/jbm.a.34081

Yang SZ, Liu YF, Feng XB, et al., 2021. HBx acts as an oncogene and promotes the invasion and metastasis of hepatocellular carcinoma both in vivo and vitro. *Dig Liver Dis*, 53(3):360-366. https://doi.org/10.1016/j.dld.2020.10.007

Yang WF, Han F, Zhang XH, et al., 2013. Extra-pulmonary tuberculosis infection in the dialysis patients with end stage renal diseases: case reports and literature review. *J Zhejiang Univ-Sci B (Biomed & Biotechnol)*, 14(1):76-82. https://doi.org/10.1631/jzus.B1200244

Yin M, Ding XR, Yin S, et al., 2023. Exosomes from hepatitis B virus-infected hepatocytes activate hepatic stellate cells and aggravate liver fibrosis through the miR-506-3p/Nur77 pathway. *J Biochem Mol Toxicol*, 37(10):e23432. https://doi.org/10.1002/jbt.23432

Zhang H, Yan XL, Guo XX, et al., 2018. MiR-27a as a predictor for the activation of hepatic stellate cells and hepatitis B virus-induced liver cirrhosis. *Oncotarget*, 9:1075-1090. https://doi.org/10.18632/oncotarget.23262

Zhao YL, Zhang S, Zhou JY, et al., 2010. The development of a tissue-engineered artery using decellularized scaffold and autologous ovine mesenchymal stem cells. *Biomaterials*, 31(2):296-307. https://doi.org/10.1016/j.biomaterials.2009.09.049

Zhou X, Zhang YL, Wang HF, et al., 2018. The development of an extra-anatomic tissue-engineered artery with collateral arteries for therapeutic angiogenesis in ischemic hind limb. *Sci Rep*, 8:4627. https://doi.org/10.1038/s41598-018-22799-4